VALIDATION AND CALIBRATION OF AN ELECTRICAL ANALOG MODEL OF HUMAN LIVER PERFUSION BASED ON HYPOTHERMIC MACHINE PERFUSION EXPERIMENTS

Running head: Calibration of a Liver Perfusion Model

Charlotte Debbaut[1], Diethard R.L. Monbaliu[2], Patrick Segers[1]

[1]Biofluid, Tissue and Solid Mechanics for Medical Applications (bioMMeda), Department of Electronics and Information Systems, iMinds Future Health Department,Ghent University, Ghent, Belgium

[2]Abdominal Transplant Surgery, University Hospitals Leuven, & Department of Microbiology and Immunology, KU Leuven, Leuven, Belgium

Corresponding author: Charlotte Debbaut, bioMMeda, Ghent University, Campus Heymans – Blok B, De Pintelaan 185, 9000 Gent, Belgium. Phone: +32 331 31 37. Email: charlotte.debbaut@ugent.be

“The Authors state that this manuscript has not been published previously and is not currently being assessed for publication by any journal other than the International Journal of Artificial Organs.”

“Each Author has contributed substantially to the research, preparation and production of the paper and approves of its submission to the Journal.”

Approval of the Institutional Review Board (IRB)/Ethics Committee was obtained for the use of human livers discarded for clinical transplantation.

Financial support: This research was supported by the Agency for Innovation by Science and Technology in Flanders (IWT; project 101115), Belgium.

There is no conflict of interest.

Presented in part during the Conference of the European Society for Artificial Organs (ESAO), September 11-14, 2013. Glasgow, United Kingdom.

ABSTRACT

Purpose: Hypothermic machine perfusion (HMP) is reviving as a better preservation method for donor livers than the golden standard of cold storage, but still faces challenges such as the risk for endothelial damage and flow competition between the arterial and portal venous inflow. Therefore, we previously developed an electrical analog model to investigate the effect of HMP settings on the human liver hemodynamics. While the model provided plausible results, it is based on a number of assumptions and its performance was never subjected to experimental validation. To this end, we present a new methodology to validate and calibrate this model to a specific liver.

Methods and results: HMP experiments were performed to capture the perfusion behavior of a human liver during varying perfusion settings. Simultaneous pressure and flow signals were acquired at the hepatic artery, portal vein and vena cava inferior. The calculation of hydraulic input impedances enabled fitting reduced Windkessel models to the global hepatic perfusion properties as an intermediate step. Based on these Windkessel models, the extended electrical analog model was calibrated to the specific available liver. Results revealed that literature values of one of the critical model parameters (wall visco-elasticity) are a few orders of magnitude off, having important consequences for simulated (pulsatile) hemodynamic variables.

Conclusion: A novel methodology, based on HMP experiments, signal processing and unconstrained nonlinear optimization, was developed to validate and calibrate the liver-specific extended electrical model. Future research may focus on extending this approach to other applications (e.g. liver pathologies such as cirrhosis).

KEYWORDS

Liver Circulation, Organ Preservation, Perfusion, Liver Transplantation, Computer Models, Computer-Assisted Signal Processing

INTRODUCTION

The substantial and continuing shortage of suitable donor livers for transplantation results in a growing usage of lower quality liver grafts, originating from extended criteria donors and donation after circulatory death donors [1]. These liver grafts are more susceptible to ischemia-reperfusion injury than standard criteria livers (originating from donation after brain death donors). Hence, hypothermic machine perfusion (HMP) has been explored as an alternative preservation method, allowing for better and longer preservation compared to cold storage [2]. Its main advantages over cold storage are a continuous supply (nutrients, drugs and oxygen) and removal (waste products and toxins) of substances, the possibility to assess graft viability, better graft survival rates etc. Previously, HMP has been shown to be the best preservation method for kidneys [3-5], while phase I studies have been conducted for livers showing that HMP provides reliable preservation [6].

Nonetheless, HMP still faces a few challenges, i.e. to avoid potential sinusoidal endothelial cell damage and heterogeneous perfusion due to flow competition between the hepatic artery (HA) and the portal vein (PV). The key question is thus how to define the optimal HMP parameter settings to maintain sufficient perfusion without inducing any damage to a given donor liver. In this context, we previously developed and published an electrical analog model of the human hepatic perfusion (Fig. 1) to investigate the effect of different HMP settings on the liver hemodynamics [7]. The model was based on equations derived from the Navier-Stokes equations by de Pater [8] and van der Plaats et al. [9]. The electrical components of the model were calculated using geometrical vascular features (branching topology, radii (r), lengths (l), numbers of vessels (n)) and pulse wave velocity values (PWV) of human liver vascular trees as acquired in [7]. A number of parameters, however, was still unknown (i.e. geometrical features of the smallest blood vessel generations and PWV values) and their values had to be estimated in order to fully define the model. Hence, it is unclear to which extent these assumptions are correct. Additional

data on the human liver perfusion are thus required to test the model-predicted results against experimental measurements.

To this end, the present study builds upon our previous work [7] in order to validate and calibrate the electrical liver model, and its aim is two-fold. The first goal was to acquire both hemodynamic and morphological data of a single human liver using HMP experiments followed by vascular corrosion casting and micro-CT scanning. Second, we aimed to develop a novel procedure to calibrate and optimize the model parameters for this specific liver by comparing model predictions to experimental data.

MATERIALS AND METHODS

This study was conducted on a human liver, which was discarded for transplantation after failed reallocation. This protocol was approved by the Ethical Committee of the University Hospitals Leuven, Belgium, and by the Belgian Liver and Intestine Committee as foreseen by the initial protocol. The methodological workflow is illustrated in Fig. 1. After receiving the donor organ, we first performed the HMP experiments to acquire hemodynamic data, after which the liver's vasculature was cast and imaged for geometrical analysis, as described before [7]. The combination of the obtained geometrical data on the liver's vasculature and its HMP data allowed calibrating an extended liver-specific electrical model. As will be described in detail below, the calibration procedure contained an intermediate step, in which the experimental data were first fitted to a reduced Windkessel model, and subsequently to the extended electrical analog model.

HMP experiment

The goal of this HMP experiment was to acquire simultaneous pressure and flow measurements at the blood inlets and outlet of the human liver (Fig. 2).

a) Liver benching

After an initial flush, the isolated liver was prepared for HMP by cannulation of the hepatic artery (HA) and the portal vein (PV) with atraumatic straight-in cannulas (Fig. 2), while a larger cannula was positioned in the suprahepatic vena cava inferior (VCI). The infrahepatic VCI was closed by a watertight suture. Subsequently, the liver was placed in the organ cassette of the HMP device, being the LifePort Workstation (Organ Recovery Systems, Zaventem, Belgium).

b) Experimental setup

While cannulating the liver graft, the HMP device and data acquisition (DAQ) equipment were prepared (Fig. 2). The tub and organ cassette of the HMP device were filled with ice water and 2 litres of KPS-1 perfusion solution (Organ Recovery Systems, Zaventem, Belgium), respectively. An oxygenator (Minimax Plus Oxygenator; Medtronic, Minnesota, USA) was included in the perfusion circuit to provide oxygenation of the perfusate (P_{O2} of 150-300 mmHg) before entering the roller pumps. Silicon tubes were used to connect the roller pumps to the HA and PV inlet cannulas. A short tube was attached to the VCI cannula to guide free fluid outflow back into the organ cassette in order to be recirculated.

Three pressure transducers (BD, New Jersey, USA) were connected to the tubing via three-way valves to perform pressure measurements as close as possible to the HA and PV inlet and the VCI outlet (Fig. 2). Before starting any measurements, all pressure transducers were zeroed to the ambient air pressure.

Flow measurements were performed by using Transonic flow meters (T206 and HT109; Transonic Systems Inc., New York, USA) together with the corresponding flow probes. Flow probes with a diameter of 5 mm, 5 mm and 9.5 mm were placed around the tubing of

the HA, PV and VCI, respectively, as close as possible to the pressure transducers to minimize potential pressure-flow signal delays.

Both pressure transducers and flow meters were connected to an SC-2345 DAQ system (National Instruments Corporation, Texas, USA) to simultaneously record all signals at a frequency of 200 Hz. A DAQ Card 6062E (National Instruments Corporation, Texas, USA) enabled reading all signals into a laptop using Labview software (National Instruments Corporation, Texas, USA). Throughout the HMP experiment, the temperature of the perfusate was kept constant at 3-8 °C and was measured by a thermometer (Ebro, Ingolstadt, Germany).

c) Measurement protocol

Perfusion settings of the HMP device were varied to investigate the liver's response. For every perfusion condition, stable perfusion parameters were awaited and measurements were recorded for at least five minutes. Pressure-controlled pulsatile perfusion without a flow limit was used for the HA, while pressure-controlled continuous perfusion with an optional flow limit was used for the PV. The initial perfusion settings were a maximum HA perfusion pressure ($P_{HA,set}$) of 25 mmHg and a maximum PV pressure ($P_{PV,set}$) of 5 mmHg (lowest achievable pump pressure) with an additional PV flow limit of ± 300 ml/min. Subsequently, these settings were repeated while varying perfusion parameters, such as increasing the $P_{HA,set}$ (to 35, 45, 55, 65, 85 and 99 mmHg).

Data analysis of the HMP experiment

Pressure and flow signals were processed using Matlab (MathWorks, Massachusetts, USA) to calculate hydraulic input impedances, which allowed fitting reduced WK models to the (global) hepatic perfusion behavior.

a) Signal processing

Flow measurements were calibrated by comparing the raw signals [V] to volumetric flow values [m^3/s], obtained by physically collecting the perfusate volume per unit of time at different flow rates. For each flow signal, a linear fit was performed to all measurement points and allowed converting the raw signals [V] to flow signals [m^3/s]. Pressure signals were corrected for pressure losses between the blood vessel in- or outlet and its pressure transducer. After calibration, pressure and flow signals were filtered to remove unwanted high frequency noise by applying a low pass third order Butterworth filter with a cut-off frequency of 15 Hz.

b) Input impedances

Hydraulic input impedance reflects the relation between pressure and flow as a function of frequency (f [Hz]). In order to calculate HA and PV input impedances, pressure and flow signals were converted from the time domain to the frequency domain by means of the discrete Fourier transformation (DFT) using the fast Fourier transform and a moving window method (time windows of 30 s with a 50 % overlap). Subsequently, the hydraulic impedances (Z) were calculated by dividing the pressure DFT by the corresponding flow DFT for all windows and taking the mean impedance over all windows. The frequency range of the reported impedances is restricted to 0-10 Hz as higher frequencies are physiologically of less importance.

Next, magnitude-squared coherences between pressure and flow signals were calculated (eq. 1 with C_{xy} the coherence, G_{xy} the cross-spectral density between signals x and y, G_{xx} and G_{yy} the autospectral densities of x and y, respectively). These coherences quantify how well pressure and flow signals are related to each other at each frequency, which allows estimating the reliability of the impedance spectra. Coherence values range

between 0 (non-related signals) and 1 (perfectly related signals). Noise, inherent to experimental measurements, may negatively affect coherence values.

$$C_{xy} = \frac{\left|G_{xy}\right|^2}{G_{xx}G_{yy}} \quad (1)$$

c) Reduced Windkessel (WK) model fitting

It is not straightforward to directly calibrate the extended electrical model to HMP-acquired data due to the limited amount and non-homogeneous distribution of coherent points and the high number of parameters to fit. Hence, we first determined the global parameters describing the hepatic perfusion using a reduced WK model, often used to model hemodynamic properties of vascular systems in a simplified way [10-13]. We choose to fit a reduced WK model configuration equal to that of the extended electrical liver model [7] and thus studied a π-element WK model (*WK*π) (Fig. 1) including a distal resistance (R_d), an inductor (L), a capacitor (C) and a component representing the visco-elasticity of the vessel walls (R_p).

HA and PV *WK*π models were fitted by minimizing the modulus difference between the *WK*π impedances (Z_{WK}) and the experimentally acquired impedances (Z). The resulting cost function (eq. 2 with $cost_{WK}$ the cost and w the weighting factor) was minimized by means of unconstrained nonlinear optimization (*fminsearch* function in Matlab).

$$cost_{WK} = \sum w\left(\left|Z_{WK}\right| - \left|Z\right|\right)^2 \quad (2)$$

Only impedance values of coherent points (C_{xy} > 0.9) were taken into account during fitting. The weighting factor w was introduced to correct for the non-homogeneous distribution of coherent points along the frequency spectrum (see for example Fig. 4): the larger the frequency difference of a coherent point to its neighboring coherent points, the higher its weight (eq. 3 with k the index of the frequency vector of coherent points).

$$w_k = f_{k+1} - f_{k-1} \quad (3)$$

Minimizing the difference between phase angles was not incorporated, as this resulted in good fitting to phase angles, but not to moduli (or vice versa). Moreover, phase angles may be unreliable due to potential time delays between pressure and flow signals.

The extended liver-specific electrical analog model

An initial electrical liver model is first obtained based solely on the acquired geometrical data. This model is then calibrated – using the reduced *WK*π model – to obtain the extended liver-specific electrical analog model.

a) Geometrical analysis to obtain an initial electrical model

Analogous to the methods in [7], a combination of vascular corrosion casting, high resolution micro-CT scanning and image processing of the human liver was performed (Fig. 1). Next, 3D reconstructions and geometrical data (branching topology, radii, lengths and numbers of vessels) of the vascular trees were acquired up to the 4th HA, PV and hepatic venous (HV) generation. Since geometrical data up to the terminal HA, PV and HV level were necessary to build an initial extended model, the measured geometrical data were extrapolated up to the terminal level (see [7, 14] for more detailed information).

All electrical components of an initial electrical analog model of the liver can now be calculated using the equations as defined in [7-9] and Fig. 1. This model is subsequently calibrated to the pressure and flow measurements via the reduced *WK*π model, as described below.

b) *Calibrating the initial electrical model*

This step involves matching the input impedances of the initial extended electrical model (Z_{EM}) to those of the $WK\pi$ model (Z_{WK}). First, vascular resistance values (R_s; Fig. 1) were adjusted (by tuning the extrapolated geometrical data with the highest degree of uncertainty) in such a way that mean pressures and flows of the model matched those measured during the HMP experiments [7]. Subsequently, the electrical components other than R_s (Fig. 1) were calibrated according to eq. 5 (with $cost_{EM}$ the cost to be minimized).

$$cost_{EM} = \sum \left(|Z_{EM}| - |Z_{WK}| \right)^2 \tag{5}$$

Using unconstrained nonlinear optimization, the optimal factors ($f_{L_{HA}}$, $f_{C_{HA}}$ and $f_{Rp_{HA}}$) were determined to multiply with the L, C and R_p values of the HA vascular tree in order to fit $|Z_{EM,HA}|$ to $|Z_{WK,HA}|$. The optimal PV factors ($f_{L_{PV}}$, $f_{C_{PV}}$ and $f_{Rp_{PV}}$) were determined in a similar way.

Pressure and flow curves (as a function of time) predicted by the electrical model were calculated by applying a sinusoidal HA source ($P_{HA} = 33 + 3\cos(2\pi f t)\left[mmHg\right]$ with t time) and a continuous PV pressure source ($P_{PV} = 4.54\left[mmHg\right]$; see also Table 1).

Sensitivity analysis of the electrical model

A parameter study was conducted on the calibrated extended liver-specific electrical model to investigate its sensitivity to changes of its electrical components. The values of all R_s, L, C or R_p components were divided and multiplied by 2 while keeping the other parameters at their calibrated values.

We also tested the effect of inducing time delays (from -20 ms to 20 ms) between pressure and flow signals, as these may arise due to practical restrictions, i.e. pressure transducers and their corresponding flow probes could not be mounted at the exact same locations.

RESULTS

HMP experiments and data analysis

a) Pressure and flow time signals

Pulsatile HA pressure (P_{HA}) and flow (Q_{HA}) signals showed repetitive fluctuations (± 1 Hz; Fig. 3a-b and e-f). PV pressure (P_{PV}) and flow (Q_{PV}) signals were more continuous, although the roller pump did induce a pulsatile component of ± 8 Hz (Fig. 3c-d and g-h). An increasing $P_{HA,set}$ resulted, as expected, in an increasing Q_{HA}, but also in an increasing P_{PV} (especially for a $P_{HA,set}$ of 65 mmHg), while the Q_{PV} decreased slightly (Fig. 3 and Table 1). P_{PV} and Q_{PV} signals gave evidence of unstable flow fluctuations for measurements with a $P_{HA,set}$ of 45 and 65 mmHg, respectively (Fig. 3c-d and g-h; starting at time stamp 1 (± 20 s) and 2 (± 70 s)), possibly indicating the onset of HA-PV flow competition (see [15] for more detailed information on this phenomenon). Interestingly, P_{HA} values only sporadically reached $P_{HA,set}$ (Fig. 3 and Table 1; especially for a $P_{HA,set}$ of 25 and 45 mmHg), most likely because the HMP feedback system measured P_{HA} near the pump outlet, while we measured P_{HA} at the actual HA inlet.

b) Input impedances

The vascular resistance (*Z(0 Hz)*; Table 1) was found consistently higher in the HA than in the PV. Z_{HA}*(0 Hz)* clearly decreased with increasing P_{HA} values, while Z_{PV}*(0 Hz)* tended to increase (especially for a $P_{HA,set}$ of 65 mmHg). HA and PV impedances are shown in Fig. 4 for a $P_{HA,set}$ of 45 mmHg and colored according to their coherence. HA coherence values were highest at the lower (0-1 Hz) and higher (6-10 Hz) end of the frequency spectrum, supplemented by a few intermediate points with relatively high coherences (near 2 and 3 Hz). This subset of coherent points shows that $|Z_{HA}|$ values seem to decline from 0-3 Hz,

followed by a gradual and slow increase up to 10 Hz. The HA phase angle (φ_{HA}) is mainly negative at low frequencies (± 0-4 Hz) and becomes positive for higher frequencies (± 4-10 Hz). $|Z_{PV}|$ values show increasing values at low frequencies (± 0-5 Hz) and approximately constant values for higher frequencies (± 5-10 Hz), while PV phase angles (φ_{PV}) followed a similar trend as φ_{HA}. However, PV impedances only showed coherent points between 0-2 Hz and near 8 Hz, implying limited frequency content in PV signals.

c) Reduced Windkessel model

HA and PV *WK*π models were fitted to the HA and PV input impedances (Fig. 5), respectively, resulting in the parameter values reported in Table 2. Since WK models were fitted solely to impedance moduli, we noted some discrepancies between fitted and measured phase angles, probably due to small time delays between pressure and flow signals (see also section “Sensitivity analysis”). Furthermore, caution is warranted when analyzing the PV *WK*π models, as PV impedances showed only a limited number of coherent points. When increasing $P_{HA,set}$, arterial perfusion properties were altered with a lower resistance to flow (decreasing R_d), lower inertial forces of the blood flow (decreasing L), a decrease in arterial buffer capacity (decreasing C) and a more outspoken visco-elastic behavior of the vessel walls (increasing R_p) (Table 2).

The extended liver-specific electrical analog model

The results in this section focus on the measurement with a $P_{HA,set}$ of 45 mmHg. Results are similar for other measurements.

a) Electrical model after calibration to R_s

The electrical model after R_s calibration results in mean flows of 105 ml/min, 233 ml/min and 338 ml/min for the HA, PV and HV vascular tree, respectively (Fig. 6a, c, e). Flow

profiles throughout the vascular trees displayed only very small changes in amplitude. HA and PV impedances of the electrical model after R_s calibration substantially differed from those of the coherent points and the $WK\pi$ model (Fig. 5). Impedance values agreed at 0 Hz, but not at higher frequencies, implying that additional calibration of L, C and R_p parameters was indeed necessary.

b) Electrical model after total calibration

The optimal factors (f_L, f_C, f_{Rp}) to fully calibrate the extended electrical model are shown in Table 3 for perfusion settings with $P_{HA,set}$ values of 25, 45 and 65 mmHg. The R_p components of the HA and PV tree as well as the L components of the PV tree had to be multiplied by a remarkably high factor in the order of 10^4 and 80-300, respectively. Increasing $P_{HA,set}$ values were associated with decreasing f_C, while f_{Rp} increased when $P_{HA,set}$ was set to 65 mmHg. No clear P_{HA}-related trend was observed for f_L.

Pressure (data not shown) and Q_{HV} curves (Fig. 6e-f) resulting from the fully calibrated model were very similar to those of the model after R_s calibration. In contrast, flow profiles of the fully calibrated model displayed substantially larger Q_{HA} amplitudes (especially for the first HA generations), while Q_{PV} amplitudes were smaller and showed time shifts (Fig. 6b, d, f). Impedance moduli of the fully calibrated model were in good agreement with the coherent points and $WK\pi$ fitted impedances (Fig. 5). Phase angles of the fully calibrated model, however, tended to underestimate the phase angles of coherent points.

Sensitivity analysis

Increased R_s values lead to higher $|Z_{HA}|$ values at 0 Hz and generally lower φ_{HA} (Fig. 7a-b). *V*ariations in L mainly affect the higher end of the frequency spectrum with higher $|Z_{HA}|$ and φ_{HA} values for higher L values (Fig. 7c-d). $|Z_{HA}|$ and φ_{HA} spectra seem to be shifted to the

left when increasing C (Fig. 7e-f). Rising R_p values give evidence of mainly higher $|Z_{HA}|$ and smaller differences between the minimum and maximum φ_{HA} (Fig. 7g-h).

We also assessed the impact of a time delay between pressure and flow signals, which mainly influences the phase angles. (Fig. 7i-j). Hence, time delays may explain the phase discrepancy between the calibrated extended electrical model and the coherent points. For example, a time delay of approximately -10 ms would make the φ_{HA} of the calibrated extended model and coherent points collide with each other.

DISCUSSION

In previous studies, we used vascular corrosion casting data to construct an electrical analog network model of a human liver. The model performance was, however, never validated to date. We therefore developed a methodology to validate and calibrate an extended electrical analog model of hepatic perfusion based on anatomical and functional data of one and the same human liver graft.

The importance of calibration for the extended electrical analog model

The impact of calibrating L, C and R_p values on the model predictions is substantial and important. This is expressed in the impedance spectra (Fig. 5), but – perhaps more tangible – in the damping of flow curves throughout the liver (Fig. 6). The fully calibrated model resulted in higher Q_{HA} and lower Q_{PV} amplitudes, showing that calibration clearly influences flow pulsations as well as the corresponding wall shear stress fluctuations, which may play a role in potential hepatic endothelial damage. The effect of calibration, however, seems most important for the larger vessels. At the sinusoidal level (microcirculation), wall shear stress fluctuation changed only from $3.57 \cdot 10^{-3}$ Pa to $3.51 \cdot 10^{-3}$ Pa after total calibration (1.7% difference).

The fully calibrated model also provides data that is better in line with in vivo measurements. Sudhamshu et al. [16] reported Doppler velocity measurements of the HA in 30 healthy patients, resulting in an estimated mean to maximal Q_{HA} ratio of 0.49. When running the electrical analog model with physiological in vivo values (a $P_{HA,set}$ with a mean value of 100 mmHg and an amplitude of 20 mmHg, a $P_{PV,set}$ of 10 mmHg), the fully calibrated extended model corresponds well with the measurements by Sudhamshu et al. and predicts a mean to maximum Q_{HA} ratio of 0.53 compared to 0.82 for the model after only R_S calibration.

The values of the electrical components of the models are, obviously, related to the radii, lengths, number of vessels and pulse wave velocity values of the blood vessel generations (see equations in Fig. 1 and [7]). In the fully calibrated model, a factor $f_{C_{HA}}$ of 17.4 was needed to calibrate the model to the data measured at an HA pressure of 45 mmHg. This corresponds to a change in *PWV* by a factor 4.17 ($=\sqrt{17.4}$) from the presumed default values, thus lowering *PWV* values from 17.7 m/s and 22.0 m/s to 4.2 m/s and 5.3 m/s for the first and terminal HA generation. These lower *PWV* values thus indicate that the initial model parameters overestimated the stiffness and also explain why the fully calibrated model displays time delays in the simulated pressure and flow waveforms as one progresses through the vessel generations (as one would expect).

The calibration procedure included an intermediate step, where we first fitted the impedance data to a reduced order $WK\pi$ model, and subsequently calibrated the extended model to the $WK\pi$ model impedance. We were forced to include this intermediate step due to a lack of sufficient coherent data points in the mid-frequency range. Direct fitting of the extended model to the measured impedance data produced model impedance spectra with unrealistic patterns in the mid-frequency range (while still fitting the data well at the low and high frequencies), which was avoided by this intermediate step.

The role of visco-elasticity (R_p values)

Model calibration shows that R_p values, and thus visco-elastic effects, were largely underestimated in the initial model (f_{Rp} correction values were in the order of 10^4). Originally, de Pater [8] introduced visco-elasticity of the vessel wall in his electrical analog model of the circulatory system using the Kelvin-Voigt model. After deriving the differential equations, it was stated that (for the case considered) the influence of R_p was unimportant, certainly for low frequencies, and that R_p could be considered constant and calculated from eq. 6.

$$R_{p1}C_1 = R_pC = 2\cdot10^{-6}\,s = 3.33\cdot10^{-8}\,\mathrm{min} \qquad (6)$$

Subsequently, van der Plaats et al. [9] used the model of de Pater to develop an electrical analog model of the dog liver, hereby applying the visco-elastic behavior of a blood vessel to the whole liver. Our data indicate that this assumption was not justified. In Fig. 8c, we plot eq. 6 together with the R_p and C values assessed in this study. Additionally, we digitized the data of Basciano et al. [17], obtained during in vivo measurements on a patient's liver, and determined R_p and C by fitting the $WK\pi$ model to the calculated impedance (Table 4 and Fig. 8a-b). The large discrepancy between the R_p versus $1/C$ relation as proposed by de Pater and the actual human liver results is obvious (Fig. 8c). Furthermore, our parameter study indicates that a change in R_p clearly affects impedance values, even for low frequencies (Fig. 7g-h), contradicting the assumption of de Pater [8] that R_p can be considered constant. We speculate that this discordance of R_p values is due to neglecting the effects of the surrounding liver tissue. It is plausible that the behavior of an isolated vessel is substantially different from that of a vessel embedded in soft liver tissue. Note also that, despite the quite drastic differences in conditions (HMP measurements versus in vivo measurements), the overall impedance patterns measured in this study and by Basciano et al. [17] agree relatively well for both livers (Fig. 8a-b).

Methodological considerations

The human liver graft used in this study was different from the liver used earlier in [7]. It was discarded for transplantation because of tumorous tissue in the kidneys and showed no signs of abnormalities or disease. The experimental procedure, starting from the hepatectomy and ending after vascular corrosion casting, was completed within 24 hours.

Clearly, the fact that the study considers only one (human) liver is a limitation. Ideally, this study should be repeated on more livers in order to clearly demonstrate perfusion behavior similarities and differences between livers. However, the procedure to obtain experimental data and build models (especially image processing and data acquisition) is very labor-intensive. In addition, human liver grafts are scarce and their availability depends on the moment that a donor organ is discarded after failed reallocation.

The acquired PV impedances showed relatively few highly coherent points (Fig. 4-5). Caution is thus recommended when interpreting the PV results. Changing the perfusion settings by inducing perturbations (such as transient phenomena, e.g. starting or stopping the pumps) or adjusting the HMP control circuit may enable generating PV data with more frequency content. HV outlet impedances were not studied, as these were not relevant due to the free outflow conditions.

Ideally, pressure and flow measurements at the sinusoids should be included to fully define the hepatic perfusion behavior. We attempted to measure sinusoidal pressures using balloon catheters which were inserted in the HV system. Unfortunately, these measurements were inaccurate and could not be included.

Future perspectives

An obvious extension of the present study is to confirm our findings in a higher number of human liver grafts, including pathological organs to gain more insight into vascular alterations affecting the hepatic hemodynamics (e.g. in cirrhosis). Since measurement

data of only the first 4 generations of blood vessels were used to generate the electrical model, the method might be applicable in vivo, using imaging data obtained with conventional MRI or CT-scanners. This may enable generating patient-specific liver models, which may turn out to be helpful in the context of surgical planning.

CONCLUSION

In this study, a novel methodology was developed to validate and calibrate an extended liver-specific electrical analog model of hepatic perfusion. The perfusion characteristics of a human liver graft were captured by performing hypothermic machine perfusion experiments and subsequently calculating hydraulic input impedances. Reduced Windkessel models were fitted to the global perfusion properties, after which their lumped properties were distributed over an electrical liver model in order to obtain a fully calibrated and extended liver-specific model. Interestingly, results revealed that literature values of one of the critical model parameters (visco-elasticity) are a few orders of magnitude off, having important consequences for simulated (pulsatile) hemodynamic variables.

Future research may focus on extending this approach from modeling HMP and natural blood flow to investigating liver pathologies and surgical procedures. Furthermore, the acquired impedances may be useful as boundary conditions for numerical models of e.g. the descending aorta, the splanchnic circulation or the portal circulation.

ACKNOWLEDGMENTS

This research was supported by the Agency for Innovation by Science and Technology in Flanders (IWT; project 101115), Belgium. The authors are grateful to the surgical team of the department of abdominal transplant surgery (University Hospitals Leuven, Belgium). Prof. dr. D. Monbaliu is holder of a chair of “Abdominal Transplant Surgery” from the “Centrale Afdeling voor Fractionering”, Vilvoorde, Belgium. B. Theunis provided excellent technical assistance. The LifePort Workstation was provided by Organ Recovery Systems, Zaventem, Belgium. The authors also want to thank prof. P. Cornillie for the vascular corrosion casting, M. Dierick and D. Van Loo for the micro-CT scanning, and Laurent Meeseman for the data processing.

REFERENCES

1. Monbaliu D, Pirenne J, Talbot D. Liver transplantation using Donation after Cardiac Death donors. *J Hepatol.* 2012;56(2):474-485.

2. Monbaliu D, Brassil J. Machine perfusion of the liver: past, present and future. *Current Opinion in Organ Transplantation.* 2010;15(2):160-166.

3. Moers C, Smits JM, Maathuis MHJ, et al. Machine perfusion or cold storage in deceased-donor kidney transplantation. *New England Journal of Medicine.* 2009;360(1):7-19.

4. Jochmans I, Moers C, Smits JM, et al. Machine perfusion versus cold storage for the preservation of kidneys donated after cardiac death: a multicenter, randomized, controlled trial. *Ann Surg.* 2010;252(5):756-764.

5. Treckmann J, Moers C, Smits JM, et al. Machine perfusion versus cold storage for preservation of kidneys from expanded criteria donors after brain death. *Transpl Int.* 2011;24(6):548-554.

6. Guarrera JV, Henry SD, Samstein B, et al. Hypothermic Machine Preservation in Human Liver Transplantation: The First Clinical Series. *American Journal of Transplantation.* 2010;10(2):372-381.

7. Debbaut C, Monbaliu D, Casteleyn C, et al. From vascular corrosion cast to electrical analog model for the study of human liver hemodynamics and perfusion. *IEEE Transactions on Biomedical Engineering.* 2011;58(1):25-35.

8. de Pater L. *An electrical analogue of the human circulatory system.* PhD dissertation. University of Groningen; Groningen, The Netherlands, 1966.

9. van der Plaats A, 't Hart NA, Verkerke GJ, et al. Numerical simulation of the hepatic circulation. *International Journal of Artificial Organs.* 2004;27(3):222-230.

10. Segers P, Rietzschel ER, De Buyzere ML, et al. Three- and four-element Windkessel models: assessment of their fitting performance in a large cohort of healthy middle-aged individuals. *Proceedings of the Institution of Mechanical Engineers Part H-Journal of Engineering in Medicine.* 2008;222(H4):417-428.

11. Stergiopulos N, Westerhof BE, Westerhof N. Total arterial inertance as the fourth element of the windkessel model. *American Journal of Physiology-Heart and Circulatory Physiology.* 1999;276(1):H81-H88.

12. Olufsen MS, Nadim A. On deriving lumped models for blood flow and pressure in the systemic arteries. *Mathematical Biosciences and Engineering.* 2004;1(1):61-80.

13. Shi Y, Lawford P, Hose R. Review of Zero-D and 1-D Models of Blood Flow in the Cardiovascular System. *Biomedical Engineering Online.* 2011;10.

14. Debbaut C, Segers P, Cornillie P, et al. Analyzing the Human Liver Vascular Architecture by Combining Vascular Corrosion Casting and Micro-CT Scanning: a Feasibility Study. *Journal of Anatomy.* In press.

15. Monbaliu D, Debbaut C, Hillewaert W, et al. Flow competition between hepatic arterial and portal venous flow during hypothermic machine perfusion preservation of porcine livers. *International Journal of Artificial Organs.* 2012;35(2):119-131.

16. Sudhamshu KC, Matsutani S, Maruyama H, Akiike T, Saisho H. Doppler study of hepatic vein in cirrhotic patients: correlation with liver dysfunction and hepatic hemodynamics. *World Journal of Gastroenteroly.* 2006;12(36):5853-5858.

17. Basciano CA. *Computational particle-hemodynamics analysis applied to an abdominal aortic aneurysm with thrombus and microsphere-targeting of liver tumors.* North Carolina State University; Raleigh, North Carolina, USA, 2010.

ABBREVIATIONS

°C	Degrees Celsius
C	Capacitor [ml/mmHg]
C_{xy}	Coherence between signals x and y
CT	Computed Tomography
DAQ	Data Acquisition
DFT	Discrete Fourier Transformation
f	Frequency [Hz]
f	Factor
G_{xx}	Autospectral density of signal x
G_{xy}	Cross-spectral density between signals x and y
HA	Hepatic Artery/Hepatic Arterial
HV	Hepatic Veins/Hepatic Venous
Hz	Hertz
HMP	Hypothermic Machine Perfusion
L	Inductor [mmHg*min²/ml]
l	Length [mm]
m	Meter
min	Minute
ml	Milliliter
mmHg	Millimeter of Mercury
n	Number of vessels
P	Pressure [mmHg]
$P_{HA,set}$	Setting of Maximal HA Pressure [mmHg]
P_{O2}	Partial Oxygen Pressure [mmHg]
$P_{PV,set}$	Setting of Maximal PV Pressure [mmHg]

PV	Portal Vein
PWV	Pulse Wave Velocity [m/s]
Q	Flow [ml/min]
r	Radius [mm]
RMSE	Root Mean Square Error
R_c	Characteristic impedance [mmHg·min/ml]
R_d	Distal resistance [mmHg·min/ml]
R_p	Visco-elasticity of the vessel wall (& surrounding liver tissue) [mmHg·min/ml]
R_s	Vascular resistance [mmHg·min/ml]
s	Second
USA	United States of America
VCI	Vena Cava Inferior
w	Weighting factor [Hz]
WK	Windkessel
WKπ	π-element Windkessel model
V	Volt
Z	Hydraulic Impedance
|Z|	Impedance Magnitude [mmHg·min/ml]
φ	Phase Angle [°]

LEGENDS

Figure 1. Methodological approach to obtain and tune an extended liver-specific electrical model.

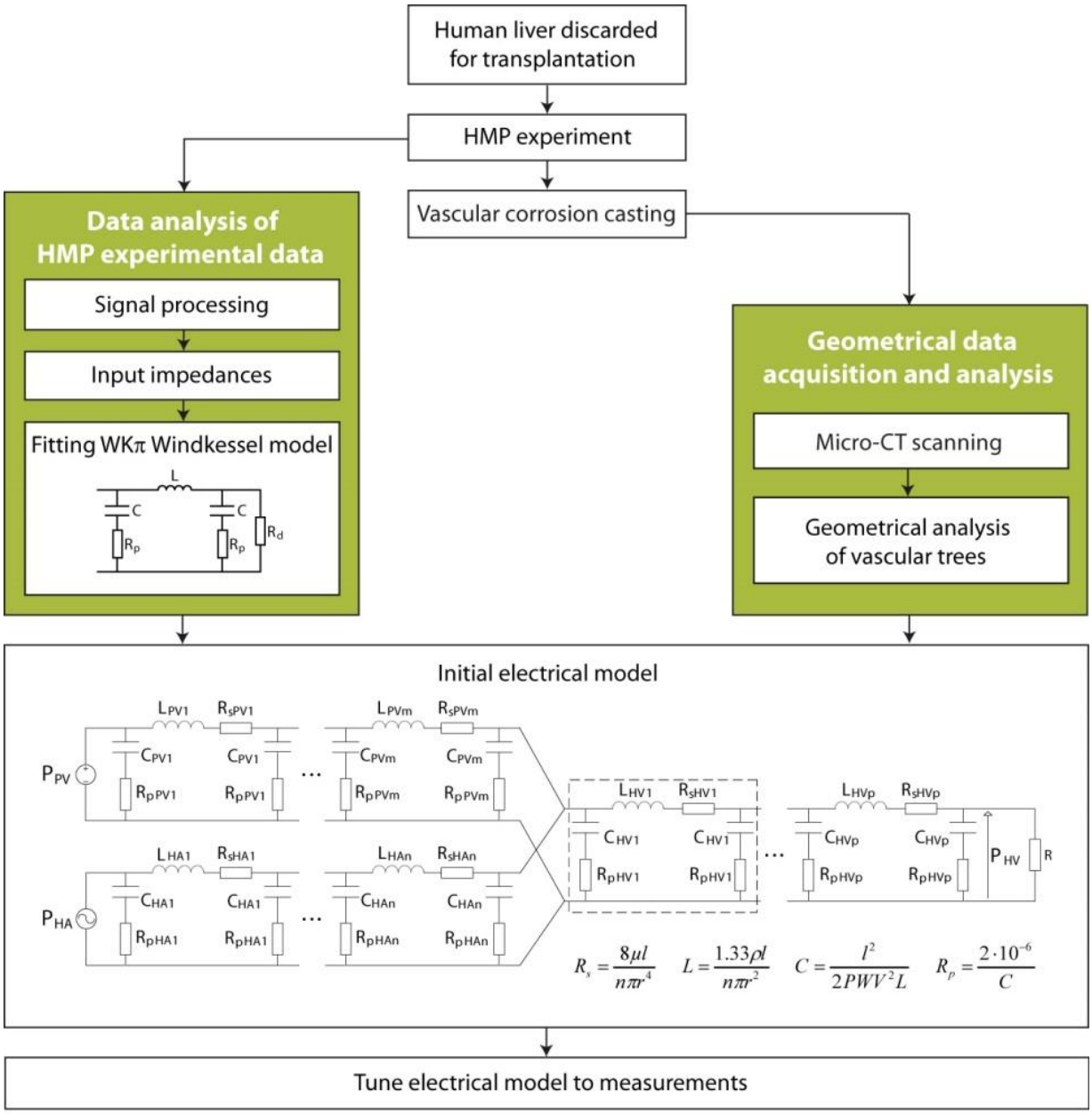

Figure 2. Experimental HMP setup: schematic overview (a) and setup (b). Two roller pumps provide inflow into the HA and PV. After leaving the liver, perfusion fluid is recirculated. Pressures and flows are measured at the HA and PV inflows and the HV outflow.

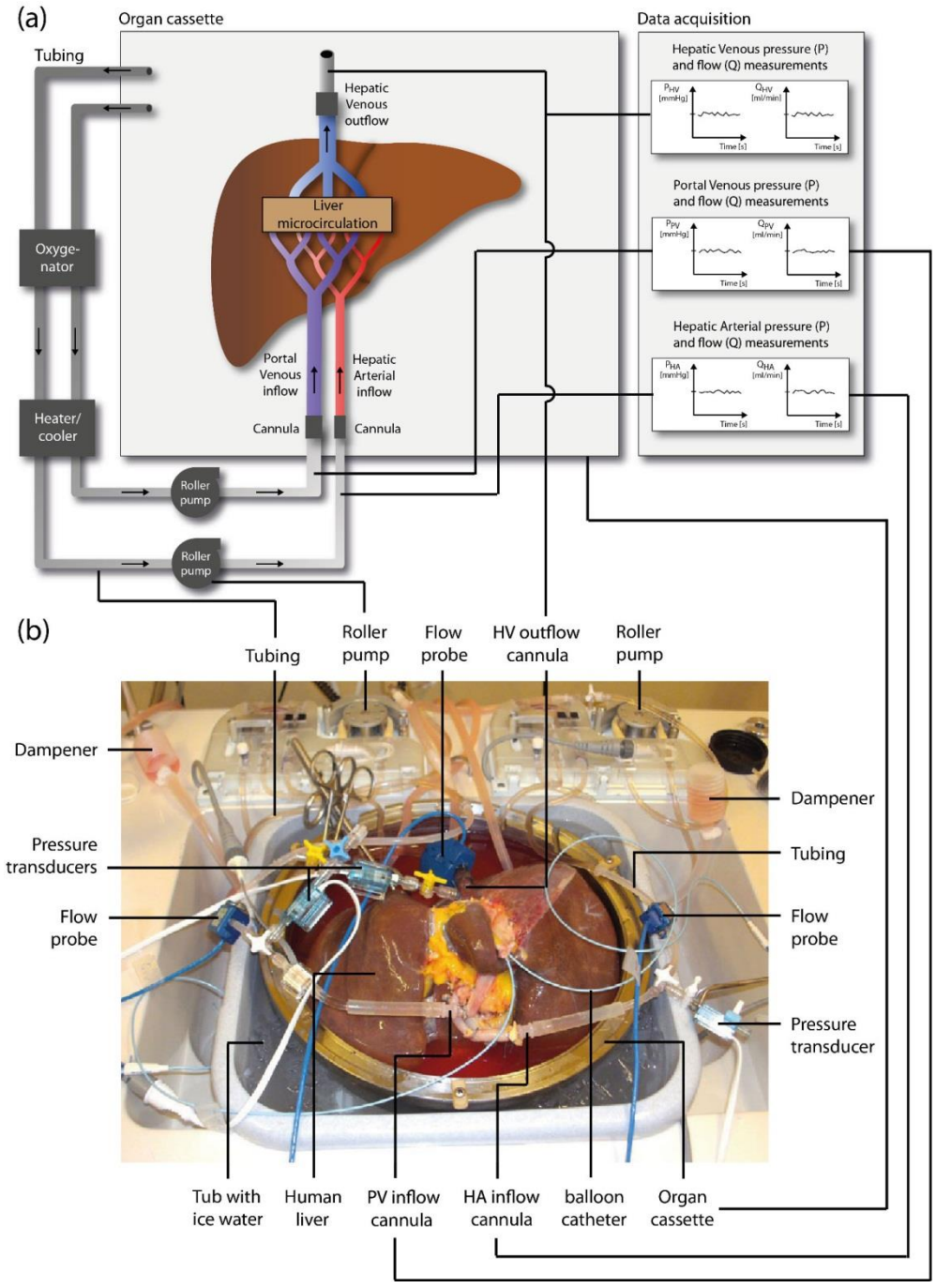

Figure 3. HA and PV pressure and flow measurements during HMP for perfusion settings with a $P_{PV,set}$ of 5 mmHg, a PV flow limit of 300 ml/min and a $P_{HA,set}$ of 25, 45, 65 mmHg, respectively. Panels a, c, e, g and b, d, f, h present measurements during 300 s and during a shorter time window of 150-200 s as indicated by boxes in panels a, c, e, g (except for the P_{PV} with a 2 s window to illustrate its inherent 8 Hz component).

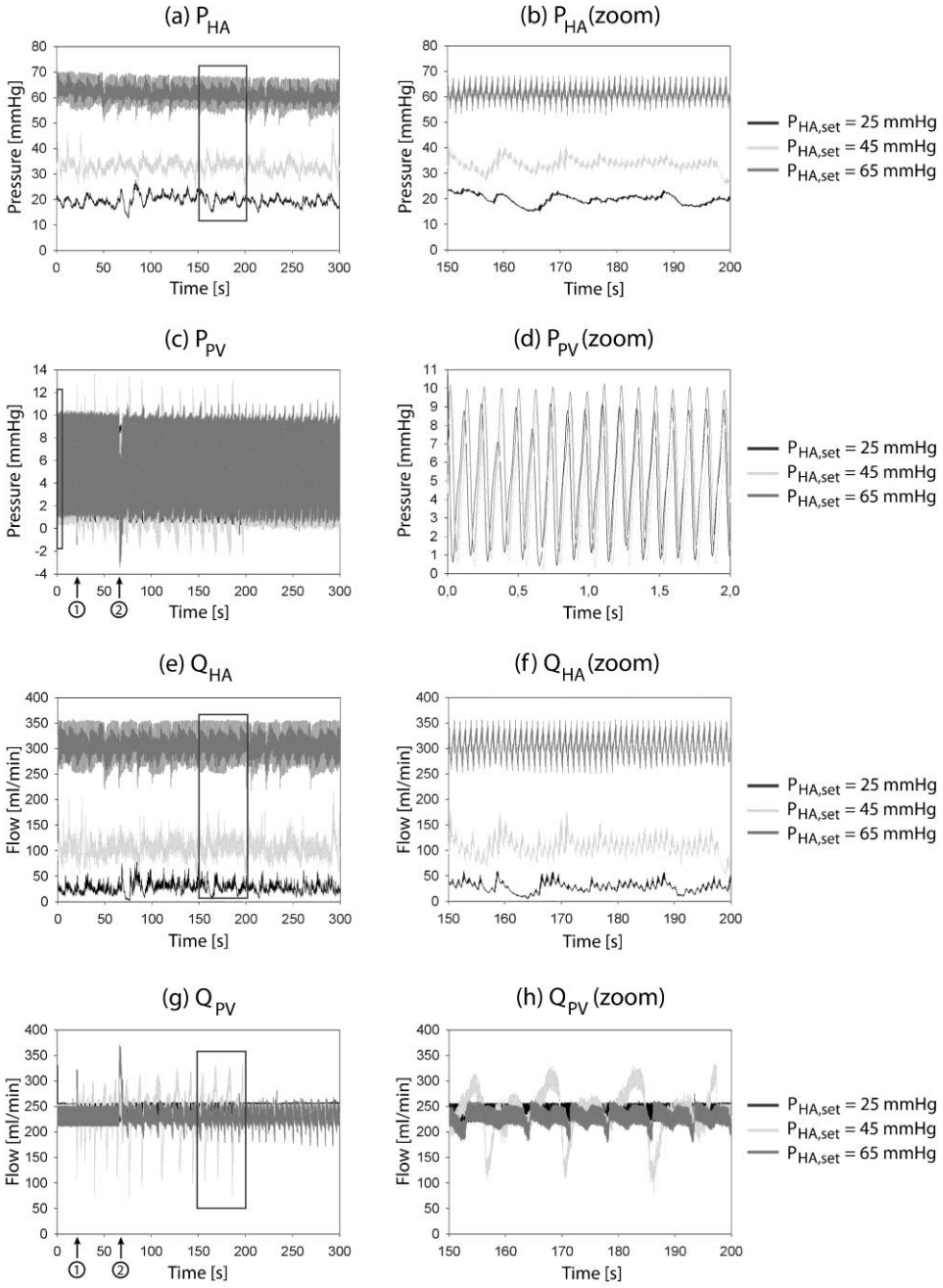

Figure 4. HA and PV input impedances of the human liver color-coded according to the coherence values for perfusion settings with a $P_{PV,set}$ of 5 mmHg, a PV flow limit of 300 ml/min and a $P_{HA,set}$ of 45 mmHg: HA and PV moduli (a, c) and phase angles (b, d).

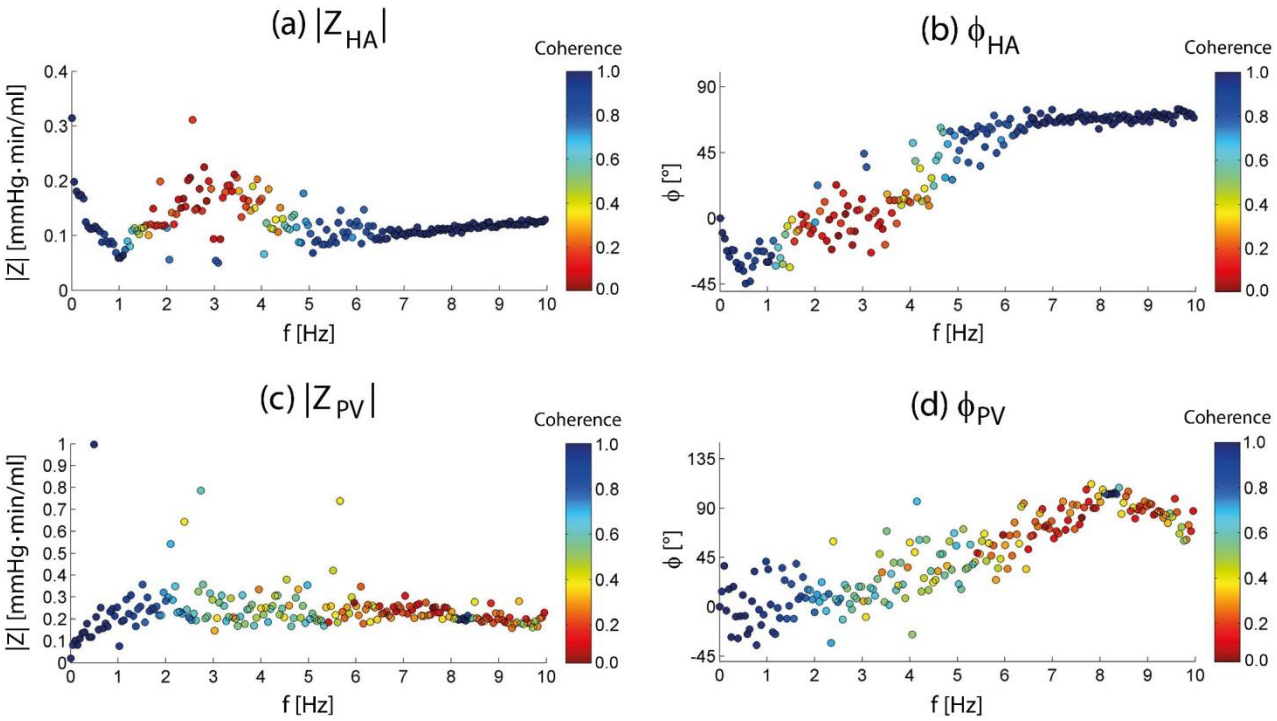

Figure 5. HA and PV input impedances of the Windkessel model and the electrical model after R_S calibration and after total calibration: HA and PV moduli (a, c) and phase angles (b, d). Coherent impedance points are also shown.

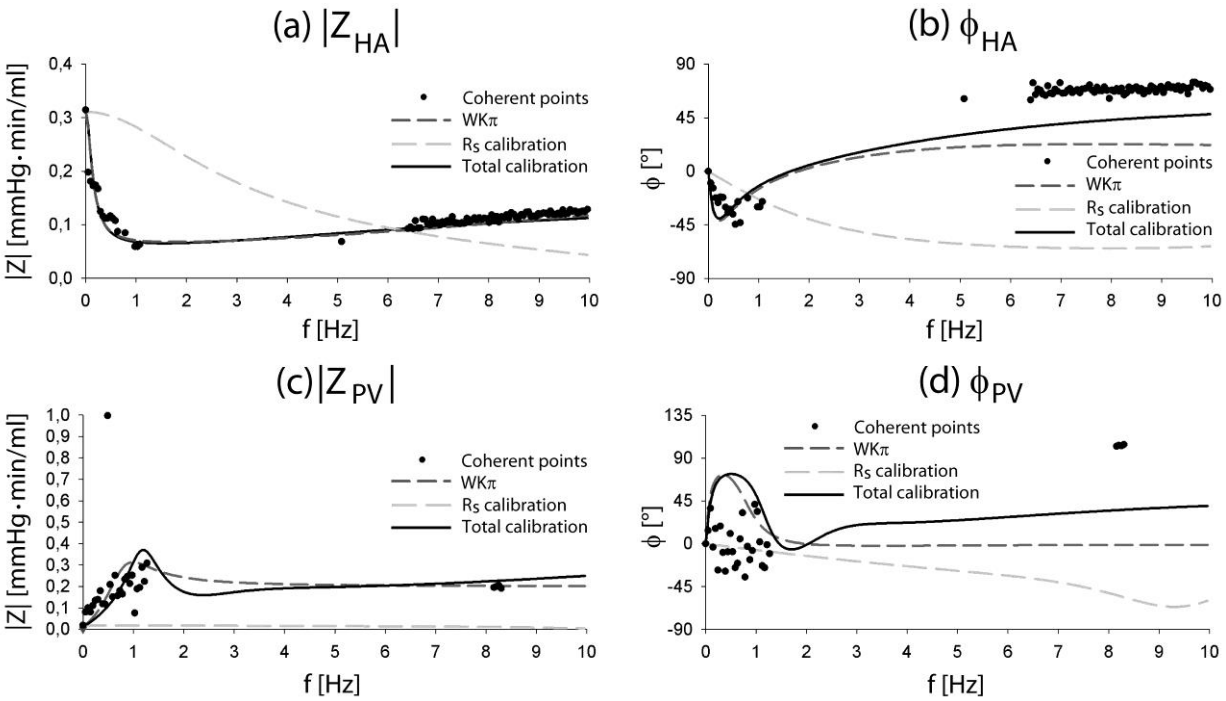

Figure 6. Time-dependent flows calculated by the electrical liver model after R_s calibration (a, c, e) and after total calibration (b, d, f): sinusoidal flows at a number of HA, PV and HV blood vessel generations.

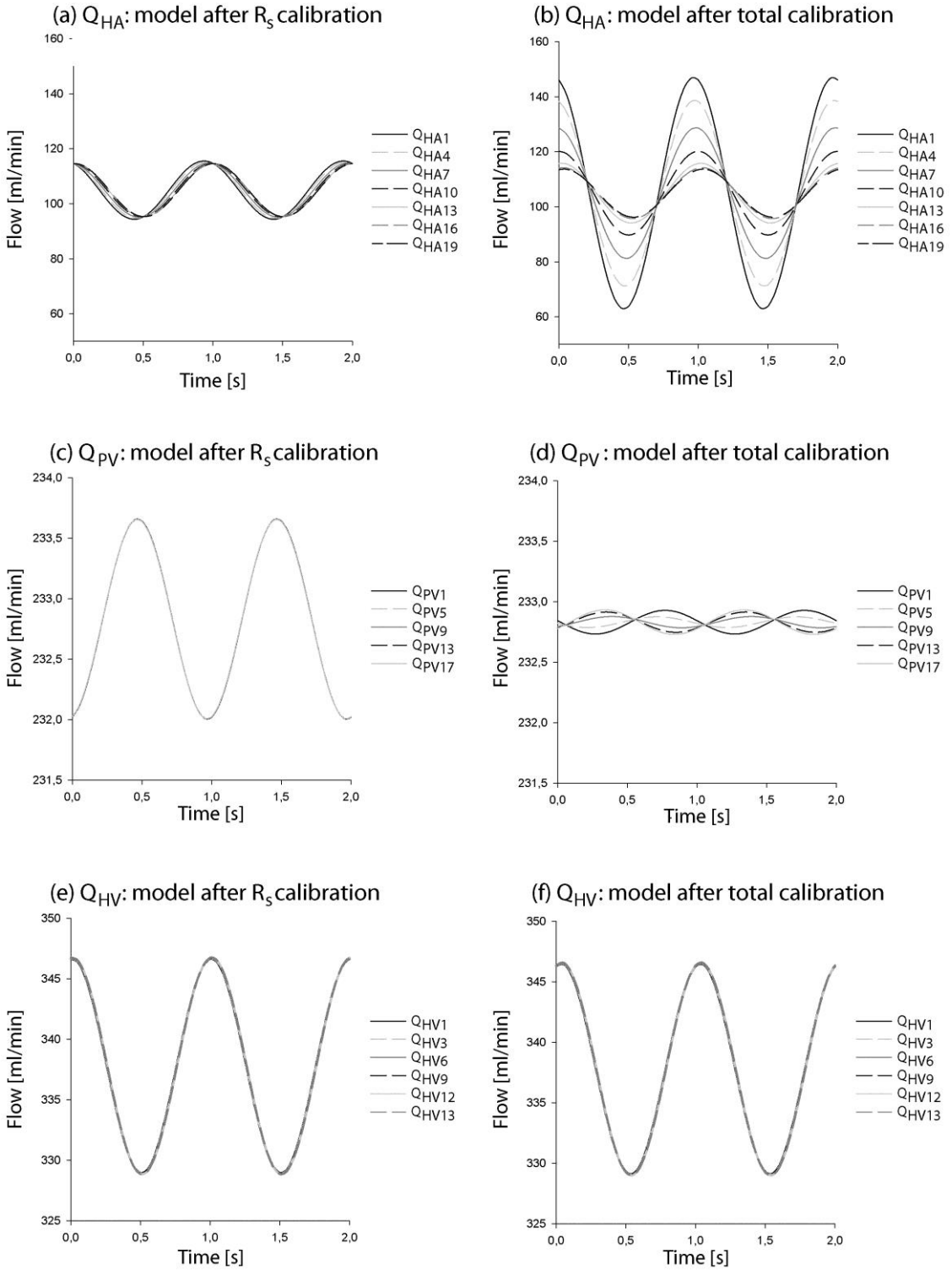

Figure 7. Results of the sensitivity analysis of the fully calibrated electrical liver model: HA impedance moduli (a, c, e, g, i) and phase angles (b, d, f, h, j) when varying R_s, L, C, R_p components and the time delay between pressure and flow signals (coherent points), respectively.

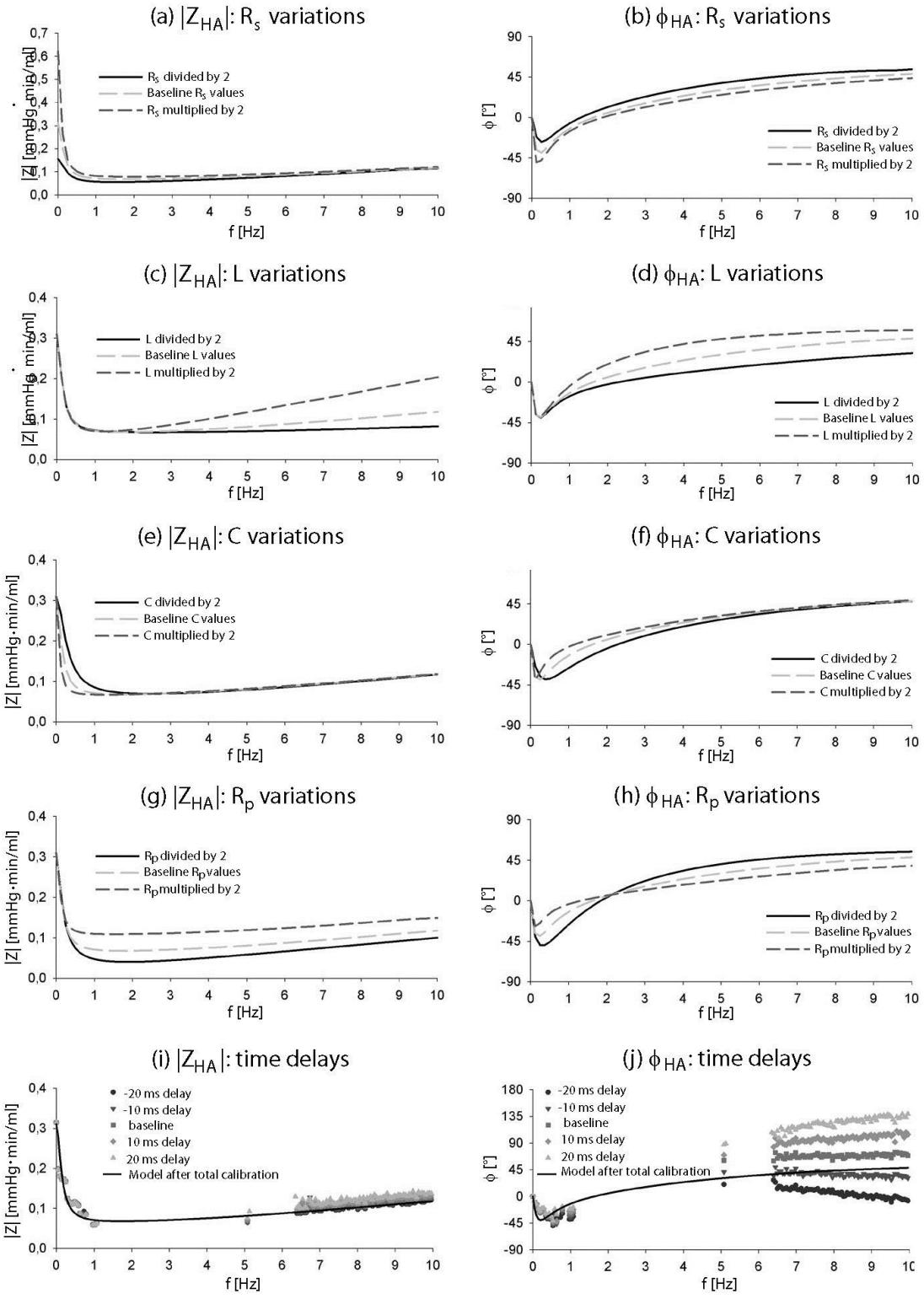

Figure 8. Comparison of the results of two human livers (our study and data of Basciano et al. [17]): (a) $|Z_{HA}|$ and (b) φ_{HA} values of coherent points and $WK\pi$ models; (c) comparison of the R_p-C relation as assumed by de Pater [8] and as calculated from the $WK\pi$ models for Z_{HA}.

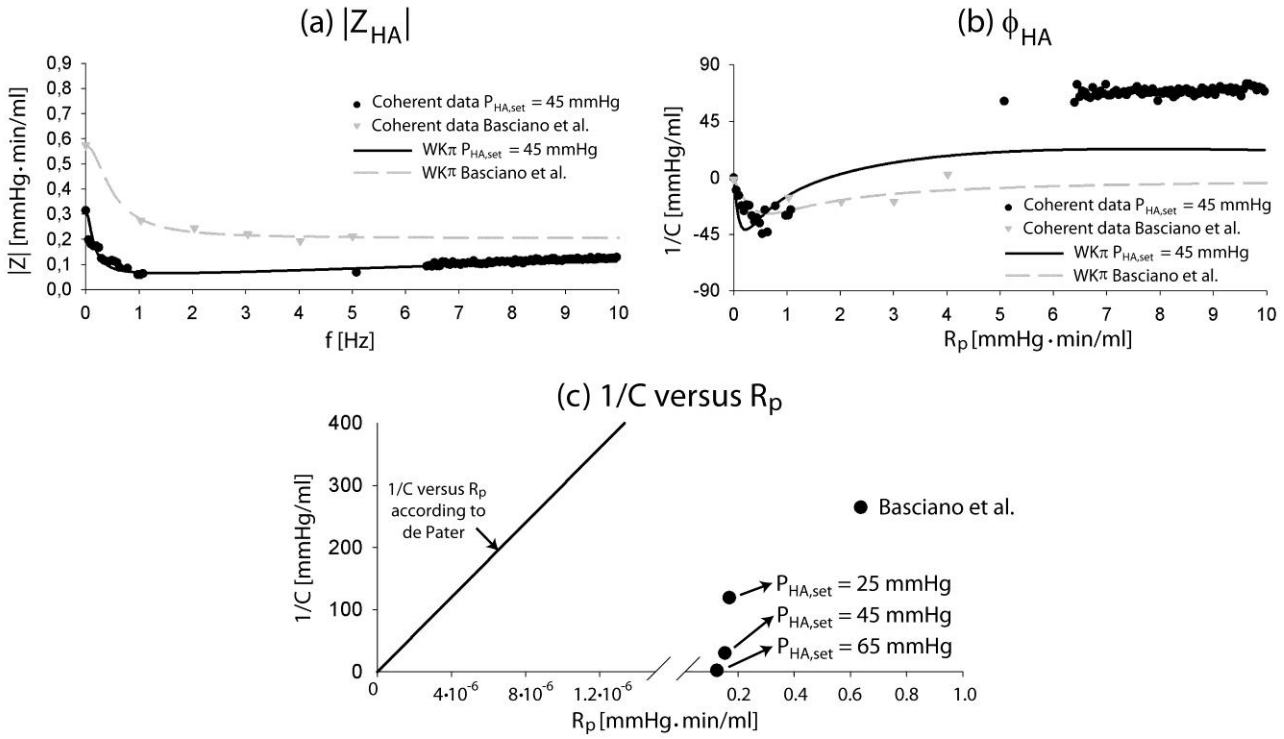

Table 1. Time-averaged pressure (*P*), flow (*Q*) and vascular resistance (*Z (0 Hz)*) values of the HMP experiments for perfusion settings with a $P_{PV,set}$ of 5 mmHg, a PV flow limit of 300 ml/min and a $P_{HA,set}$ of 25, 45 and 65 mmHg, respectively.

$P_{HA,set}$ [mmHg]	P_{HA} [mmHg]	P_{PV} [mmHg]	Q_{HA} [ml/min]	Q_{PV} [ml/min]	Z_{HA}(0 Hz) [mmHg*min/ml]	Z_{PV}(0 Hz) [mmHg*min/ml]
25	19.7	4.69	27.8	236	$7.07 \cdot 10^{-1}$	$1.99 \cdot 10^{-2}$
45	33.0	4.54	105	233	$3.14 \cdot 10^{-1}$	$1.95 \cdot 10^{-2}$
65	60.5	5.35	303	228	$2.00 \cdot 10^{-1}$	$2.35 \cdot 10^{-2}$

Table 2. Electrical components of the WK models fitted to the HA and PV impedances for perfusion settings with a $P_{PV,set}$ of 5 mmHg, a PV flow limit of 300 ml/min and a $P_{HA,set}$ of 25, 45 and 65 mmHg (only 45 mmHg for the PV), respectively. The corresponding root mean square errors (RMSE) are also given.

	$P_{HA,set}$ [mmHg]	R_d [mmHg* min/ml]	L [mmHg* min²/ml]	C [ml/ mmHg]	R_p [mmHg* min/ml]	$RMSE$ [mmHg* min/ml]
HA	**25**	$7.11 \cdot 10^{-1}$	$1.46 \cdot 10^{-4}$	$4.47 \cdot 10^{-1}$	$1.25 \cdot 10^{-1}$	$3.19 \cdot 10^{-2}$
HA	**45**	$3.14 \cdot 10^{-1}$	$6.05 \cdot 10^{-5}$	$3.31 \cdot 10^{-2}$	$1.53 \cdot 10^{-1}$	$1.61 \cdot 10^{-2}$
HA	**65**	$2.00 \cdot 10^{-1}$	$5.55 \cdot 10^{-5}$	$8.38 \cdot 10^{-3}$	$1.68 \cdot 10^{-1}$	$1.82 \cdot 10^{-2}$
PV	**45**	$1.95 \cdot 10^{-2}$	$6.84 \cdot 10^{-4}$	$1.38 \cdot 10^{-2}$	$2.00 \cdot 10^{-1}$	$1.68 \cdot 10^{-1}$

Table 3. Results of the electrical liver model calibration: f_L, f_C, f_{Rp} factors and *RMSE* values for both the HA and PV fitted to their corresponding *WK*π models (for perfusion settings with a $P_{PV,set}$ of 5 mmHg, a PV flow limit of 300 ml/min and a $P_{HA,set}$ of 25, 45 and 65 mmHg, respectively).

$P_{HA,set}$ [mmHg]	f_{LHA}	f_{CHA}	f_{RpHA}	$RMSE_{HA}$ [mmHg*min/ml]	f_{LPV}	f_{CPV}	f_{RpPV}	$RMSE_{PV}$ [mmHg*min/ml]
25	4.03	26.0	$9.40 \cdot 10^{3}$	$9.2 \cdot 10^{-3}$	273	2.51	$1.36 \cdot 10^{4}$	$4.3 \cdot 10^{-2}$
45	3.51	17.4	$9.29 \cdot 10^{3}$	$2.3 \cdot 10^{-3}$	292	1.82	$1.33 \cdot 10^{4}$	$3.6 \cdot 10^{-2}$
65	3.65	4.15	$1.23 \cdot 10^{4}$	$2.2 \cdot 10^{-3}$	80.8	1.40	$2.82 \cdot 10^{4}$	$3.8 \cdot 10^{-3}$

Table 4. *WK*π models fitted to the $|Z_{HA}|$ values of two human livers. The *WK*π model of the human liver was fitted to HMP acquired $|Z_{HA}|$ values for perfusion settings with a $P_{HA,set}$ of 45 mmHg. The *WK*π model based on the data of Basciano et al. [17] was fitted to patient-specific in vivo measurements. Fitted parameters and *RMSE* and *Rp·C* values are reported. (Remark: The *L* value based on the data of Basciano et al. [17] is unreliable as *L* mainly affects the high frequency response and no reliable high frequency data were available for fitting of this liver.)

	R_d [mmHg*min/ml]	L [mmHg*min²/ml]	C [ml/mmHg]	R_p [mmHg*min/ml]	*RMSE* [mmHg*min/ml]	$R_p \cdot C$ [mmHg*min/ml]
$P_{HA,set}$ of 45 mmHg	$3.14 \cdot 10^{-1}$	$6.05 \cdot 10^{-5}$	$3.31 \cdot 10^{-2}$	$1.53 \cdot 10^{-1}$	$1.61 \cdot 10^{-2}$	$5.06 \cdot 10^{-3}$
Basciano et al.	$5.75 \cdot 10^{-1}$	$2.16 \cdot 10^{-10}$	$3.78 \cdot 10^{-3}$	$6.36 \cdot 10^{-1}$	$1.04 \cdot 10^{-2}$	$2.40 \cdot 10^{-3}$